


Article

Cyclic Hot Corrosion Failure Behaviors of EB-PVD TBC Systems in the Presence of Sulfate and Vanadate Molten Salts

Yasin Ozgurluk ^{1,*}, Kadir Mert Doleker ¹, Dervis Ozkan ², Hayrettin Ahlatci ³ 
and Abdullah Cahit Karaoglanli ¹

¹ Department of Metallurgical and Materials Engineering, Faculty of Engineering, Bartin University, 74100 Bartin, Turkey; mertdoleker@gmail.com (K.M.D.); cahitkaraoglanli@gmail.com (A.C.K.)

² Department of Mechanical Engineering, Faculty of Engineering, Bartin University, 74100 Bartin, Turkey; dervisozkan@gmail.com

³ Department of Metallurgical and Materials Engineering, Faculty of Engineering, Karabuk University, 78050 Karabuk, Turkey; hahlatci@karabuk.edu.tr

* Correspondence: ozgurlukyasin@gmail.com

Received: 28 January 2019; Accepted: 20 February 2019; Published: 1 March 2019



Abstract: The cold gas dynamic spray (CGDS) method has been considered a promising technology to produce a metallic bond coat for thermal barrier coating (TBC) systems. In this study, CoNiCrAlY bond coats produced by CGDS method were coated with yttria-stabilized zirconia (YSZ) by electron beam physical vapor deposition (EB-PVD). TBCs were subjected to 50 wt % V₂O₅ and 50 wt % Na₂SO₄ molten hot corrosion salt combinations at 1000 °C. In the case of YSZ top coat on TBCs, the reaction between Na₂SO₄, V₂O₅, and Y₂O₃ salts generates YVO₄ crystals, and these structures cause the transformation of tetragonal ZrO₂ to monoclinic ZrO₂. This situation occurs under operating conditions that lead to TBC failure. Hot corrosion behavior and the related failure mechanisms of TBC systems were investigated and discussed using scanning electron microscope (SEM), energy dispersive spectroscopy (EDS) analysis, and X-ray diffractometer (XRD).

Keywords: thermal barrier coatings (TBCs); electron beam physical vapor deposition (EB-PVD); cold gas dynamic spray (CGDS); hot corrosion; molten salts

1. Introduction

Thermal barrier coatings (TBCs) have been widely used to improve the efficiency of gas turbine engines in aviation industry [1–3]. Mostly, aircraft engines work at elevated temperatures, and these temperatures generally damage aircraft engine parts, such as turbines and blades. TBCs have been used in gas turbine engine components, like turbine blades and vanes, to protect them from aggressive environmental effects, increase operating temperatures, and provide thermal insulation at higher operating temperatures [4,5].

Yttria-stabilized zirconia (YSZ) is widely used as a traditional TBC ceramic top coat material due to its high melting point, low thermal conductivity, and high-temperature stability. MCrAlY alloy is also used as a typical TBC bond coat material due to its excellent high-temperature strength [1,2,4]. When TBCs are exposed to oxidation with high temperature, a thermally grown oxide (TGO) layer is formed between the top coat and bond coat [6]. The ceramic top coat has a substantially low thermal conductivity and partially low thermal expansion. The metallic bond coat is deposited between the metallic substrate and ceramic top coat for improving adherence of the ceramic top coating to the substrate alloy [7].

Bond coats are an important part of TBCs, and they can be produced by a variety of methods such as atmospheric plasma spray (APS), vacuum plasma spray (VPS), high-velocity oxy-fuel (HVOF), or cold gas dynamic spray (CGDS) [8]. CGDS is a thermal spraying technique by which the powder coating materials are deposited on the surface at high speeds at considerably lower process temperatures. This high-speed process is carried out by heating and compressing gases such as air, nitrogen, and helium. The CGDS method has many advantages over other thermal spray coating methods. The products produced by this method do not cause undesirable phase structures and oxidation. There is no change in the structure of the base material. It is also possible to obtain dense and high-hardness coatings. CGDS coatings can be produced at very high speeds. The most important advantage of this method is that CGDS method is applied at lower temperatures than other thermal spray coating processes, such as HVOF, APS, and D-gun [1,8]. CGDS technique may appear to be an alternative process to obtain superior coating properties for bond coat production. CGDS coatings, commonly known as “cold spray” coatings, exhibit remarkably high density, good corrosion resistance, and high hardness with high reliability, due to their cold-worked microstructure [9]. Cold-sprayed bond coats show improved adhesion to the substrate and provide a suitable surface roughness [10].

Ceramic top coat production is the most important part of TBC production. Generally, two methods are available for this purpose, namely, APS and EB-PVD. EB-PVD coatings are deposited in a columnar structure as opposed to APS coatings which grow in a laminar manner. EB-PVD has a more complex mechanism than plasma spraying, in terms of the equipment used. EB-PVD methods need preheating for the substrate while for plasma spray methods, it is not necessary to heat the substrate and the coating rate is faster than EB-PVD. APS is a low-cost, easy, and rapid production technique compared to EB-PVD. In addition, EB-PVD TBCs have good aerodynamic properties due to their surface roughness, which is better than APS [11].

TBCs undergo a variety of failure mechanisms, such as hot corrosion, oxidation, erosion, and thermal shock. Thermal shock occurs with sudden temperature alterations. Oxidation occurs as a result of chemical reactions of metallic components at high temperatures. Hot corrosion is the most important failure mechanism in TBC. Hot corrosion takes place due to the adverse effects of molten salts at high temperature [12]. In a working gas turbine, sulfur which comes from the low-quality fuel reacts with sodium chloride and sodium sulfate forms at high temperatures. After that, sodium sulfate covers the hot-section components. This phenomenon is commonly referred to as “hot corrosion”. Turbine blade alloys that suffer hot corrosion attack have been widely found to show both oxidation and sulfidation [10]. This occurs at high temperature and in corrosive environments. However, this mechanism has not been exactly declared due to the use of low-quality fuels. Some low-quality fuels have impurities, such as Na_2SO_4 and V_2O_5 salts, covering the component surface at the high temperature. These salts reacting with the top coat cause phase transformation [1]. As a result, this transformation causes volume expansion and, accordingly, failure occurs depending on the TBC system [12].

In this study, the CGDS method, widely used as a novel technology in recent years, was used to deposit CoNiCrAlY-based metallic bond coats onto nickel-based superalloy substrate Inconel 718. EB-PVD method was used for deposition of ceramic top coatings with YSZ content, which are used for thermal insulation purposes. The primary aim of this study is the deposition of CoNiCrAlY-based metallic bond coats having a dense structure with low oxide and porosity content. Another aim is evaluation of the failure mechanisms and performances occurring under high temperature and corrosion conditions in EB-PVD TBC systems.

2. Experimental

2.1. Preparation of Substrate Material, and Bond and Top Coatings

Inconel 718, a nickel-based superalloy, was used as the substrate material. The approximate dimensions of 1 inch diameter and 4 mm thickness were obtained by cutting with wire erosion process.

Sample surfaces were prepared by sandblasting for the coating process. The deposition of CoNiCrAlY metal powders was accomplished with CGDS technique. Approximately 100 μm coating thickness was achieved on nickel-based superalloy substrate material. Following the production of bond coat, the deposition of top coat was accomplished with nearly 300 μm thickness by EB-PVD technique using YSZ ceramic-based ingots. In the EB-PVD unit for deposition of top coating, YSZ ingot material of 68.5 mm diameter and 45–55 mm height was used.

2.2. Hot Corrosion Tests

Salt mixtures of Na_2SO_4 (99% purity) and V_2O_5 (98% purity) were scattered onto the surfaces of produced TBC samples. The corrosive salts were spread over the surface of specimens at a concentration of 10 mg/cm^2 , keeping 1.5 mm from the edge to avoid edge effects. The samples were subjected to hot corrosion tests at 1000 $^\circ\text{C}$ (1273 K) temperature, with periodical cycling between furnace and room temperature for 4 h periods. These cycles were continued until about 40% deterioration was observed on the samples. After each 4 h period of testing at 1000 $^\circ\text{C}$, the samples were allowed to cool down inside the furnace, and the coatings were then inspected for possible crack initiation. The samples were then recoated with the $\text{Na}_2\text{SO}_4 + \text{V}_2\text{O}_5$ salt mixture.

2.3. Characterization

Microstructures of TBCs were evaluated using a scanning electron microscope (SEM) (SEM, Tescan, MAIA3 XMU, Brno, Czech Republic) equipped with latest technology energy dispersive spectroscopy (EDS-SEM, Tescan, MAIA3 XMU). The phases of the TBCs were analyzed using X-ray diffraction (XRD) (Rigaku Dmax 2200 PC, Cu $K\alpha$ radiation, Tokyo, Japan). Surface roughness values were measured using the surface roughness tester (SJ-310, Mitutoyo, Kanagawa, Japan). Hardness values of the coatings were measured using Vickers indentation using a Struers Duramin microhardness tester (Copenhagen, Denmark) with 100 g load for 15 s periods. Corrosive product formation and degradation mechanisms were examined using surface and cross-sectional microstructural analysis. The important results of this study are presented in this paper.

3. Results and Discussion

3.1. Characterization of as-Sprayed Coatings

Substrate material, metallic bond, and ceramic top coat's surface roughness were measured according to DIN EN ISO 3274 standard [13], and are shown in Table 1. Metallic bond coats, which were produced by CGDS methods, had dense, little porosity, and uniform structure [1,6,11].

Table 1. Surface roughness values of substrate, and bond and top coat.

Surface Roughness	R_a (μm)
Inconel-718 substrate	5.25
CGDS bond coat	7.20
EB-PVD top coat	7.92

The bond coat cross-section of the as-deposited EB-PVD TBCs with cold-sprayed CoNiCrAlY bond coat is demonstrated in Figure 1. As observed in the image, the coating exhibits a columnar structure, which is a typical feature of EB-PVD coating [1–5,14–17]. The TBC structure produced with EB-PVD method has a lower crack content. As-deposited TBC surface image is shown in Figure 2. The top surface of the coating exhibits a pyramidal appearance and intercolumnar gaps can be observed.

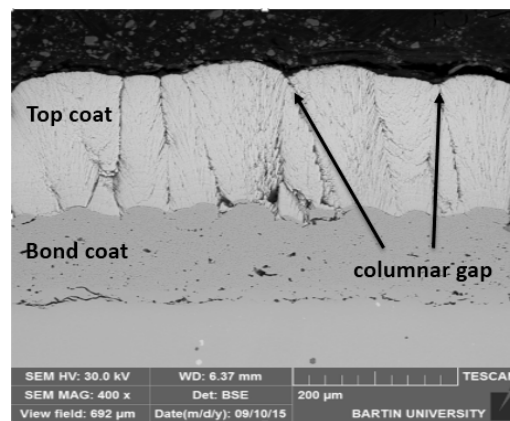


Figure 1. As-deposited cross-sectional microstructure of yttria-stabilized zirconia (YSZ) thermal barrier coating (TBC) system.

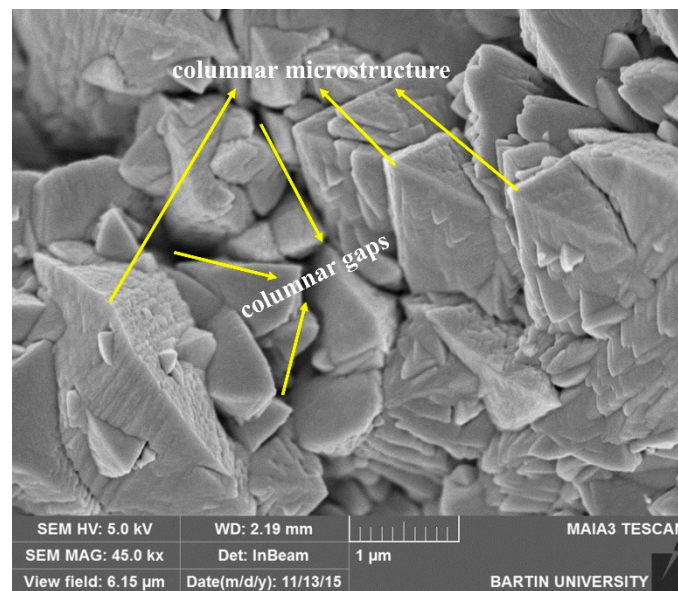


Figure 2. As-deposited columnar surface image micrograph of microstructure of YSZ TBC.

After hot corrosion tests, a uniform and dense coating structure provided by EB-PVD technique retards the formation of hot corrosion products [1,5,8,12]. The substrate material, metallic bond, and ceramic top coat surface hardness values are given in Table 2.

Table 2. Hardness values of the thermal barrier coating component.

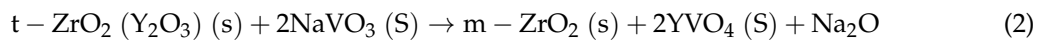
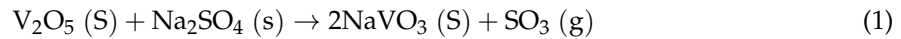
Material	Hardness Values (H_v)
Inconel-718	203.9
CoNiCrAlY Bond Coat	407.9
YSZ Top Coat	713.8

3.2. Effect of Hot Corrosion on TBC Samples

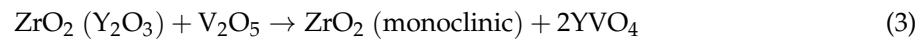
Effects of hot corrosion occurred due to molten salts leaking from the microcracks and porosities in the top layer. Elements, such as sodium and vanadium, lead to a change in the phase structure of YSZ top coating layer in service conditions. If Na, S, P, V, etc. elements exist in structure due to fuel pollution, they can react with the Y_2O_3 phase. Tetragonal–monoclinic phase transformation in stabilized ZrO_2 happens in the absence of Y_2O_3 phase. This transformation causes both structural

integrity deterioration and volumetric change [16,17]. Reaction of melted sulfate and vanadium salts is needed to completely understand the damage mechanism of hot corrosion on YSZ [11].

The process of hot corrosion has been emphasized in several earlier studies [1,6,11,14,15]. The hot corrosion action can be expressed by the following reactions [1,6,14,18,19].



The below reaction can also directly occur [1,6,14,18].



During the hot corrosion on TBCs, yttria slowly runs out. After depletion of yttria, the transformation from tetragonal zirconia to monoclinic zirconia during the cooling step of thermal cycling occurs by 3%–5% volume expansion, leading to cracking and spallation of TBCs [1,4,6,8,20].

A cross-section SEM image of EB-PVD TBC with cold-sprayed CoNiCrAlY bond coat after 20 h hot corrosion test is shown in Figure 3. No evidence of reaction was found between YSZ and Na_2SO_4 in the XRD results. However, Na_2SO_4 shows a faster effect of chemical reaction in hot corrosion mechanism [1,10,16,21]. Moreover, the presence of NaVO_3 increases the mobility of Y^{3+} . Thus, exhaustion of yttria and growth of YVO_4 crystal is enhanced [7]. It is accepted that YSZ usually stabilizes in tetragonal phase due to the presence of Y_2O_3 . For this reason, in the case of a decrease in Y_2O_3 , tetragonal ZrO_2 phase turns into monoclinic ZrO_2 phase [21–23]. At the interface between YSZ ceramic top coating and CoNiCrAlY metallic bond coating, TGO layer and surface cracks were formed. In addition, the EB-PVD TBCs exposed to hot corrosion salts exhibited spallation of the top coat near the bond coat/top coat interface. Monoclinic ZrO_2 and YVO_4 crystals caused wide crack formation in the YSZ ceramic top coating.

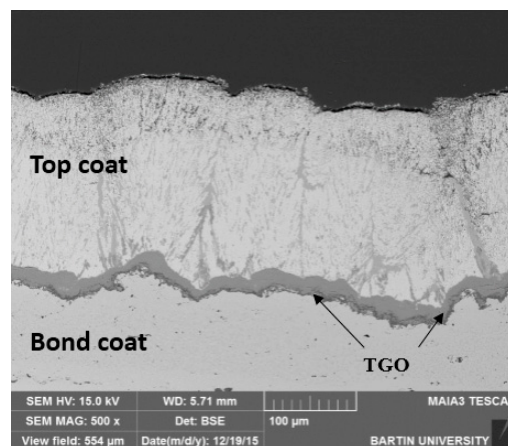


Figure 3. Cross-sectional microstructure of YSZ TBC after the hot corrosion test.

Following the hot corrosion test, closure of the porous structure was observed among the columns. This situation is attributed to the sintering effect and decreasing of spaces among the columns. When the undesirable effect of sintering appears as a damaging factor in TBC systems, decreased elongation tolerance at high temperatures due to increasing mechanical properties of the coating and consequent spallation damage occur [24–29]. After the 20 h hot corrosion test, the hot corrosion tests were stopped due to the separation of coating from the coating surface.

EB-PVD TBC surface image and EDS analysis after 20 h hot corrosion tests are respectively given in Figures 4 and 5. YVO_4 rod crystals in YSZ coating were revealed after hot corrosion. After the hot corrosion test, structures of rod-shaped crystals according to EDS and XRD analyses were identified

with the formation of YVO_4 phases [6,21]. It was revealed that YSZ ceramic top coating consisted of a porous surface and a few rod crystals. The rod-shaped structures generally form as columnar boundaries on TBC samples. Y_2O_3 reacted with V_2O_5 and after this reaction, YVO_4 rod-shaped structures occurred on TBC samples [6].

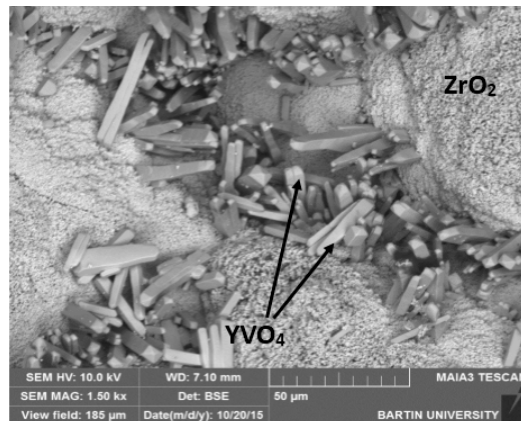


Figure 4. Surface microstructure of TBC after the hot corrosion test.

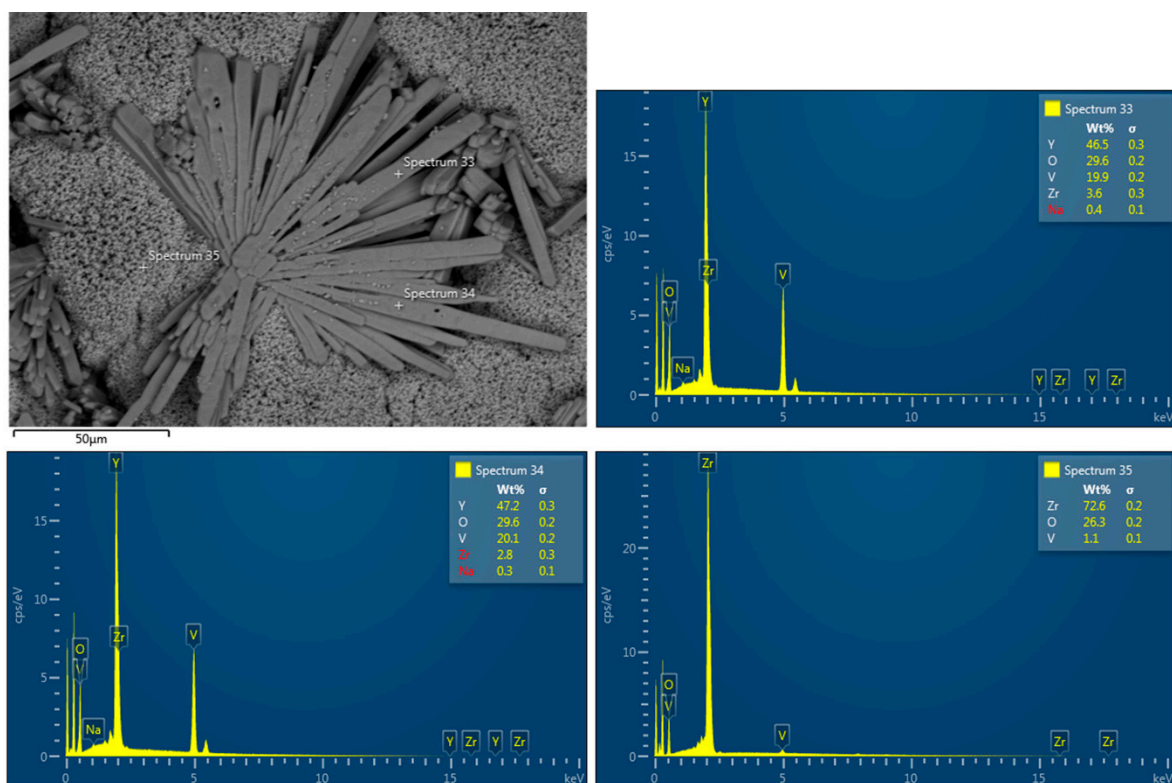


Figure 5. Surface microstructure with EDS analysis of YSZ TBC after the hot corrosion test.

In particular, due to the fact that columnar structure is denser and has less porosity, penetration of hot corrosion molten salts hardly occurred on the columnar microstructured TBCs. When the molten salts can easily penetrate from the top coat, a hot corrosion mechanism quickly occurs. Hot corrosion molten salt products, such as vanadium, oxygen, and yttria, can be seen in the cross-sectional image and surface image after hot corrosion tests. Hot corrosion products can be seen considering the surface image of samples in EDS analysis. Moreover, hot corrosion products can be seen in elemental mapping analysis (Figure 6) after hot corrosion test. According to that figure, oxygen coincides with vanadium and yttrium. It can be understood from this analysis that rod-shaped YVO_4 crystals were detected as

one of the hot corrosion products. In addition to the EDS and elemental mapping analyses, the XRD phase analysis in Figure 7 demonstrates that monoclinic ZrO_2 phase is also another hot corrosion product besides the YVO_4 phase. Before the hot corrosion test, the top coat has only tetragonal ZrO_2 phase. After the 20 h hot corrosion test, top coat spallation occurs as a result of phase transformation.

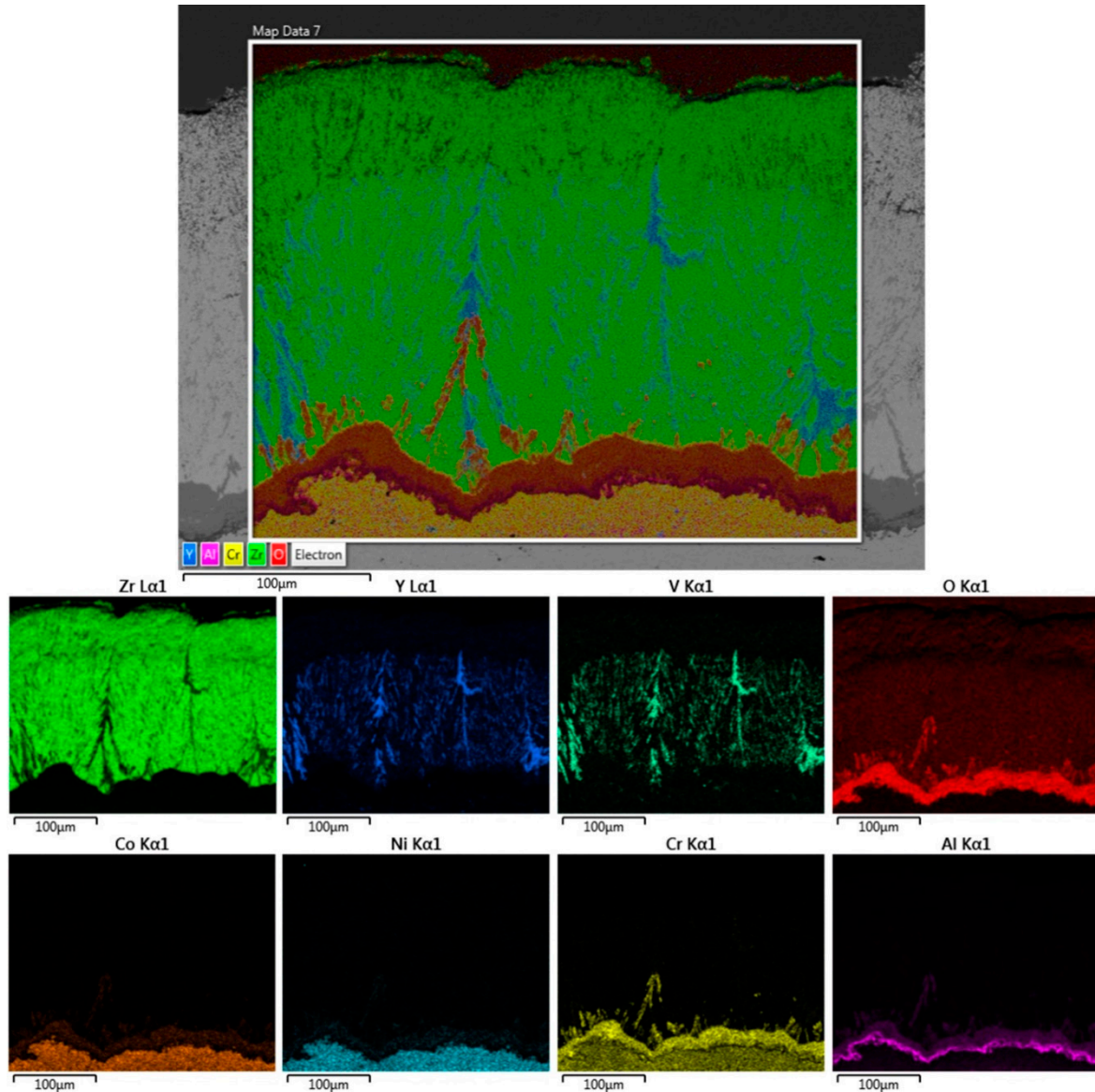


Figure 6. Cross-sectional microstructure with elemental mapping analysis belonging to TBC system after the hot corrosion test.

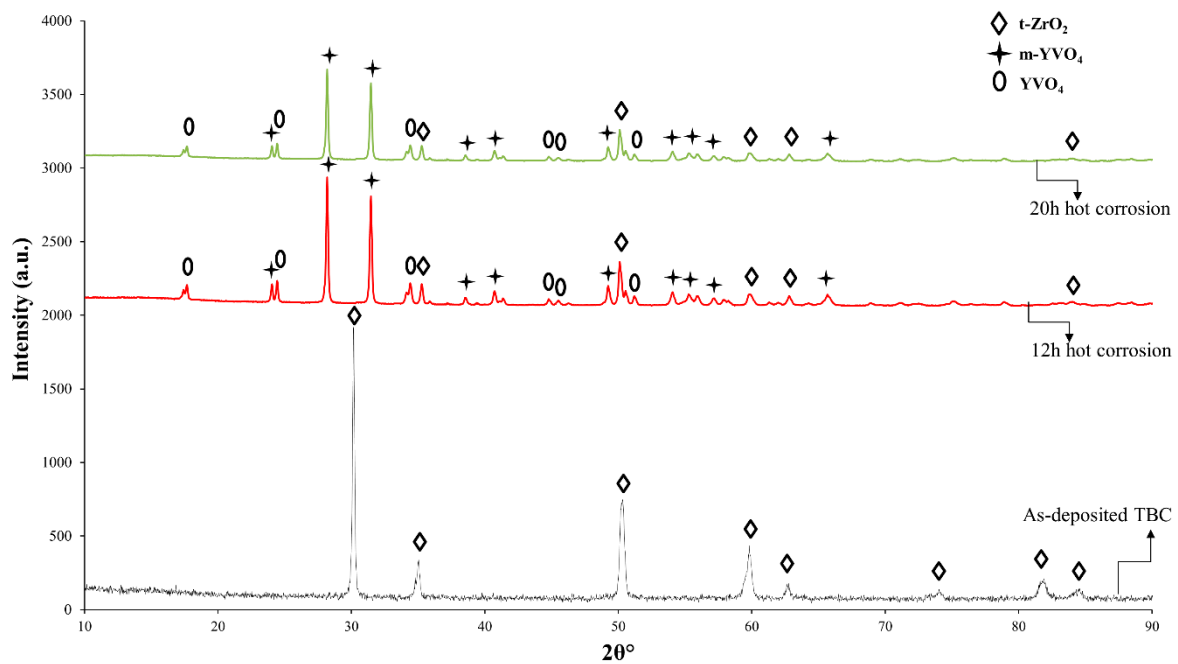


Figure 7. XRD analysis of TBC before and after hot corrosion tests.

During 22, 42, and 100 h hot corrosion tests in $\text{Na}_2\text{SO}_4 + \text{V}_2\text{O}_5$ salt mixture environment, formation of YVO_4 crystals were observed as hot corrosion products [5,6,16,23]. In similar studies conducted with YSZ top coating in $\text{Na}_2\text{SO}_4 + \text{V}_2\text{O}_5$ salt mixture environment as molten salt, phase transformation-related spallations were observed on top coatings of TBC samples, in spite of varying number and duration of cycles [1,6,16,21]. Due to the melting point of $\text{Na}_2\text{SO}_4 + \text{V}_2\text{O}_5$ salt mixture, about 900°C , and that our test temperature is above this temperature, this salt mixture become molten during the test [18]. Hui et al. stated in their research [7] that after SEM, XRD, and EDS analyses, YVO_4 formations with rod-shaped crystal structure were observed as a result of isothermal hot corrosion tests with 6, 12, 24, 48, and 96 h time periods that were conducted at 1100°C in a Na_2SO_4 -30 mol % NaVO_3 environment. YVO_4 phases were only observed in 48 and 96 h periods, while monoclinic ZrO_2 was observed in all hot corrosion test periods according to XRD analysis. However, YVO_4 phases were obtained throughout each cycle in our present study. This may be related to the presence of V_2O_5 in our hot corrosion salts.

Liu et al. [30] observed a volumetric increase in thermal barrier coating samples comprising of Sc_2O_3 - Y_2O_3 - ZrO_2 (ScYSZ) subjected to hot corrosion test at 1000°C in a $\text{Na}_2\text{SO}_4 + \text{V}_2\text{O}_5$ environment, which was attributed to the phase transformation of zirconium dioxide, from tetragonal to monoclinic phase [1,7,11,16,19,21]. This phase transformation caused crack formation in the coating. After the hot corrosion tests, it was determined that ScYSZ had a longer lifetime compared to YSZ. It is stated that the presence of less yttria in ScYSZ influences this situation. After corrosion tests of ScYSZ, phase transformation occurred in the coating structure, but no YVO_4 phase formation was observed. The EB-PVD TBC system provides a high elongation tolerance under thermal loads. This ensures that the thermal cycle lifetime of EB-PVD TBCs is longer than APS. However, the molten corrosion salts leaking from the columnar openings progress more rapidly. For this reason, while expansion columns are closing, corrosion products that react with the surfaces found here have an accelerating effect on the damage of the coating. In solutions of precursor plasma spray (SPSS), there are similar columnar openings. Ajay et al. [18] stated that in the case of the TBC samples produced with SPSS and APS methods, and tested in 90% $\text{Na}_2\text{SO}_4 + 5\% \text{V}_2\text{O}_5 + 5\% \text{NaCl}$ environment and 50% $\text{Na}_2\text{SO}_4 + 50\% \text{V}_2\text{O}_5$ environment at 900°C , the sample produced with APS method exhibited a higher cycle life compared to the one produced with another method in both environments [3,14,21]. In other research [1,6,16,21,26] at higher temperatures such as 1050 and 1100°C , and lower temperatures such

as 950 °C, formations of rod-shaped YVO_4 were also observed in YSZ top coatings. However, in top coating materials other than YSZ, such as $Gd_2Zr_2O_7$ and Ta_2O_5 , failures were observed in the form of spallations rather than rod-shaped formations like YVO_4 [1,6,16,21]. When Wang et al. [31] investigated $La_2Ce_2O_7$ /YSZ thermal barrier double layer coatings, hot corrosion molten salts penetrated into the microcolumnar gap and reacted with La element. After the reaction of molten salt with La element, the top coating microstructure of $La_2Ce_2O_7$ deteriorated because of the formation of $CeVO_4$ and $LaVO_4$. In comparison with $La_2Ce_2O_7$, YSZ was not affected by the chemical reaction of molten salts. $La_2Ce_2O_7$ stopped the progression of corrosive salts to YSZ [31]. Xu and others [32] used rare earth zirconates $La_2Zr_2O_7$ and $La_2(Zr_{0.7}Ce_{0.3})_2O_7$ to produce TBCs with EB-PVD method. TBC samples were subjected to hot corrosion test by holding them for 100 h in molten salt solution. In the XRD analyses performed after the hot corrosion tests, monoclinic zirconia and YVO_4 phases were found to be similar to our study. In a study conducted by Xu et al. [32], La_2O_3 served as a stabilizer in the coating. After the hot corrosion test, La_2O_3 within the structure was separated from the structure due to reaction with $NaVO_3$. Y_2O_3 reacted with $NaVO_3$ formed by molten salts and formed YVO_4 structure. This reaction led to tetragonal to the monoclinic phase transformation of the top coat. These reactions caused the damage in the top coat. Similar damage can be seen in this study [32].

Gavendova et al. [33] produced TBC coatings with CGDS and HVOF techniques, and reported that the interdendritic structure of the CGDS bond coats included more porosity as compared to those produced with HVOF method. Reportedly, the phase and chemical composition of HVOF bond coat was better than that of the CGDS bond coat. As opposed to Gavendova et al. [33], Khanna and Rathod [34] reported that CGDS coatings exhibited better wear and friction behavior than HVOF coatings. Owing to the low process temperatures of CGDS method, substrate materials do not undergo unfavorable structural changes during the deposition process. However, in their study on HVOF and CGDS, Khanna and Rathod showed that the coatings produced by the CGDS method showed better wear and friction behavior than the coatings produced by the HVOF method. As a result, the strength of the overall TBC system can be maintained by use of this method.

4. Conclusions

In the present work, the hot corrosion behavior of a new generation of TBC system, including a CoNiCrAlY bond coat and an 8YSZ top coat, was studied, and the following conclusions are drawn:

- The structure of metallic bond coat produced with CGDS technique was found to have a denser structure with lower porosity and oxide content due to the production characteristics of the process.
- Along with the hot corrosion effect, the formation of TGO was also observed on the specimens, since the furnace environment in which the hot corrosion tests were conducted was open to the atmosphere.
- The EDS analyses indicate that formations of rod crystal structures observed in the microstructural images obtained from the top surface of TBC systems belong to YVO_4 crystals. Chemical reactions of $NaVO_3$, forming as a result of the reaction of Y_2O_3 , Na_2SO_4 , and V_2O_5 salts penetrating into YSZ top coating, also contributed to the formation of YVO_4 crystals.
- The molten salts that leaked from the top coating caused deterioration of the structure with the columnar openings provided by EB-PVD, which played a role in accelerating damage. At the end of the hot corrosion tests, it was determined that the columnar structure was destroyed.
- Along with the YVO_4 crystals in rod form, the reasons underlying the failure of coatings in TBC systems were found to be volumetric changes and transformations at the rate of 3%–5% during the cooling process of ZrO_2 , which has been transformed into monoclinic phase structure from tetragonal phase structure.

Author Contributions: A.C.K., Y.O., K.M.D., H.A. and D.O. designed the experiments; A.C.K. and Y.O. performed the experiments; A.C.K., Y.O., and K.M.D. analyzed the data; A.C.K., Y.O. and K.M.D. wrote, reviewed and edited the paper.

Funding: This research was funded by The Scientific and Technological Research Council of Turkey, TUBITAK, 113R049.

Acknowledgments: The authors thank H.E. (from Bartın University) for his support on characterization of samples.

Conflicts of Interest: The authors declare no conflict of interest.

References

1. Ozgurluk, Y.; Doleker, K.M.; Karaoglanli, A.C. Hot corrosion behavior of YSZ, Gd₂Zr₂O₇ and YSZ/Gd₂Zr₂O₇ thermal barrier coatings exposed to molten sulfate and vanadate salt. *Appl. Surf. Sci.* **2018**, *438*, 96–113. [[CrossRef](#)]
2. Sreedhar, G.; Raja, V.S. Hot corrosion of YSZ/Al₂O₃ dispersed NiCrAlY plasma-sprayed coatings in Na₂SO₄–10 wt.% NaCl melt. *Corros. Sci.* **2010**, *52*, 2592–2602. [[CrossRef](#)]
3. Eliaz, N.; Shemesh, G.; Latanision, R.M. Hot corrosion in gas turbine components. *Eng. Fail. Anal.* **2002**, *9*, 31–43. [[CrossRef](#)]
4. Clarke, D.R.; Levi, C.G. Materials design for the next generation thermal barrier coatings. *Annu. Rev. Mater. Res.* **2003**, *33*, 383–417. [[CrossRef](#)]
5. Karaoglanli, A.C.; Doleker, K.M.; Demirel, B.; Türk, A.; Varol, R. Effect of shot peening on the oxidation behavior of thermal barrier coatings. *Appl. Surf. Sci.* **2015**, *354*, 314–322. [[CrossRef](#)]
6. Habibi, M.H.; Wang, L.; Guo, S.M. Evolution of hot corrosion resistance of YSZ, Gd₂Zr₂O₇, and Gd₂Zr₂O₇ + YSZ composite thermal barrier coatings in Na₂SO₄ + V₂O₅ at 1050 °C. *J. Eur. Ceram. Soc.* **2012**, *32*, 1635–1642. [[CrossRef](#)]
7. Hui, Y.; Zhao, S.; Xu, J.; Zou, B.; Wang, Y.; Cai, X.; Zhu, L.; Cao, X. High-temperature corrosion behavior of zirconia ceramic in molten Na₂SO₄ + NaVO₃ salt mixture. *Ceram. Int.* **2016**, *42*, 341–350. [[CrossRef](#)]
8. Moy, C.K.S.; Cairney, J.; Ranzi, G.; Jahedi, M.; Ringer, S.P. Investigating the microstructure and composition of cold gas-dynamic spray (CGDS) Ti powder deposited on Al 6063 substrate. *Surf. Coat. Technol.* **2010**, *204*, 3739–3749. [[CrossRef](#)]
9. Kuzmichew, A.; Tsybulski, L. Evaporators with induction heating and their applications. In *Advances in Induction and Microwave Heating of Mineral and Organic Materials*; Grundas, S., Ed.; IntechOpen: London, UK, 2011; pp. 269–302.
10. Burlacov, I.; Jirkovský, J.; Kavan, L.; Ballhorn, R.; Heimann, R.B. Cold gas dynamic spraying (CGDS) of TiO₂ (anatase) powders onto poly(sulfone) substrates: Microstructural characterisation and photocatalytic efficiency. *J. Photochem. Photobiol. A Chem.* **2007**, *187*, 285–292. [[CrossRef](#)]
11. Wahl, G.; Metz, C.; Samoilenkov, S. Thermal barrier coatings. *J. Phys. IV France* **2001**, *11*, Pr3-835–Pr3-846. [[CrossRef](#)]
12. Jiang, S.M.; Peng, X.; Bao, Z.B.; Liu, S.C.; Wang, Q.M.; Gong, J.; Sun, C. Preparation and hot corrosion behaviour of a MCrAlY + AlSiY composite coating. *Corros. Sci.* **2008**, *50*, 3213–3220. [[CrossRef](#)]
13. *ISO 3274:1996 Geometrical Product Specifications (GPS)—Surface Texture: Profile Method—Nominal Characteristics of Contact (Stylus) Instruments*; International Organization for Standardization: Geneva, Switzerland, 1996.
14. Afrasiabi, A.; Saremi, M.; Kobayashi, A. A comparative study on hot corrosion resistance of three types of thermal barrier coatings: YSZ, YSZ + Al₂O₃ and YSZ/Al₂O₃. *Mater. Sci. Eng. A* **2008**, *478*, 264–269. [[CrossRef](#)]
15. Habibi, M.H.; Wang, L.; Liang, J.; Guo, S.M. An investigation on hot corrosion behavior of YSZ-Ta₂O₅ in Na₂SO₄ + V₂O₅ salt at 1100 °C. *Corros. Sci.* **2013**, *75*, 409–414. [[CrossRef](#)]
16. Daroonparvar, M.; Yajid, M.A.M.; Yusof, N.M.; Bakhsheshi-Rad, H.R.; Hamzah, E.; Nazoktabar, M. Investigation of three steps of hot corrosion process in Y₂O₃ stabilized ZrO₂ coatings including nano zones. *J. Rare Earths* **2014**, *32*, 989–1002. [[CrossRef](#)]
17. Mensch, A.; Thole, K.A.; Craven, B.A. Conjugate heat transfer measurements and predictions of a blade endwall with a thermal barrier coating. *J. Turbomach.* **2014**, *136*, 121003. [[CrossRef](#)]

18. Ajay, A.; Raja, V.S.; Sivakumar, G.; Joshi, S.V. Hot corrosion behavior of solution precursor and atmospheric plasma sprayed thermal barrier coatings. *Corros. Sci.* **2015**, *98*, 271–279. [[CrossRef](#)]
19. Mifune, N.; Harada, Y.; Doi, T.; Yamasaki, R. Hot-corrosion behavior of graded thermal barrier coatings formed by plasma-spraying process. *J. Therm. Spray Technol.* **2004**, *13*, 561–569. [[CrossRef](#)]
20. Mobarra, R.; Jafari, A.H.; Karaminezhaad, M. Hot corrosion behavior of MCrAlY coatings on IN738LC. *Surf. Coat. Technol.* **2006**, *201*, 2202–2207. [[CrossRef](#)]
21. Levi, C.G.; Vidal-Sétif, M.H.; Johnson, C.A.; Hutchinson, J.W. Environmental degradation of thermal-barrier coatings by molten deposits. *MRS Bull.* **2012**, *37*, 932–941. [[CrossRef](#)]
22. Tsai, P.C.; Lee, J.H.; Hsu, C.S. Hot corrosion behavior of laser-glazed plasma-sprayed yttria-stabilized zirconia thermal barrier coatings in the presence of V_2O_5 . *Surf. Coat. Technol.* **2007**, *201*, 5143–5147. [[CrossRef](#)]
23. Li, S.; Liu, Z.G.; Ouyang, J.H. Growth of $YbVO_4$ crystals evolved from hot corrosion reactions of $Yb_2Zr_2O_7$ against V_2O_5 and $Na_2SO_4 + V_2O_5$. *Appl. Surf. Sci.* **2013**, *276*, 653–659. [[CrossRef](#)]
24. Yugeswaran, S.; Kobayashi, A.; Ananthapadmanabhan, P.V. Hot corrosion behaviors of gas tunnel type plasma sprayed $La_2Zr_2O_7$ thermal barrier coatings. *J. Eur. Ceram. Soc.* **2012**, *32*, 823–834. [[CrossRef](#)]
25. Feuerstein, A.; Knapp, J.; Taylor, T.; Ashary, A.; Bolcavage, A.; Hitchman, N. Technical and economical aspects of current thermal barrier coating systems for gas turbine engines by thermal spray and EB-PVD: A review. *J. Therm. Spray Technol.* **2008**, *17*, 199–213. [[CrossRef](#)]
26. Ghasemi, R.; Shoja-Razavi, R.; Mozafarinia, R.; Jamali, H. The influence of laser treatment on thermal shock resistance of plasma-sprayed nanostructured yttria stabilized zirconia thermal barrier coatings. *Ceram. Int.* **2014**, *40*, 347–355. [[CrossRef](#)]
27. Saremi, M.; Valefi, Z.; Abaeian, N. Hot corrosion, high temperature oxidation and thermal shock behavior of nanoagglomerated YSZ–alumina composite coatings produced by plasma spray method. *Surf. Coat. Technol.* **2013**, *221*, 133–141. [[CrossRef](#)]
28. Kotlan, J.; Ctibor, P.; Pala, Z.; Homola, P.; Nehasil, V. Improving dielectric properties of plasma sprayed calcium titanate ($CaTiO_3$) coatings by thermal annealing. *Ceram. Int.* **2014**, *40*, 13049–13055. [[CrossRef](#)]
29. Mohan, P. Environmental Degradation of Oxidation Resistant and Thermal Barrier Coatings for Fuel-Flexible Gas Turbine Applications. Ph.D. Thesis, University of Central Florida, Orlando, FL, USA, May 2010.
30. Liu, H.F.; Xiong, X.; Li, X.B.; Wang, Y.L. Hot corrosion behavior of Sc_2O_3 – Y_2O_3 – ZrO_2 thermal barrier coatings in presence of $Na_2SO_4 + V_2O_5$ molten salt. *Corros. Sci.* **2014**, *85*, 87–93. [[CrossRef](#)]
31. Wang, X.; Guo, L.; Peng, H.; Zheng, L.; Guo, H.; Gong, S. Hot-corrosion behavior of a $La_2Ce_2O_7$ /YSZ thermal barrier coating exposed to $Na_2SO_4 + V_2O_5$ or V_2O_5 salt at 900 °C. *Ceram. Int.* **2015**, *41*, 6604–6609. [[CrossRef](#)]
32. Xu, Z.; He, L.; Mu, R.; He, S.; Huang, G.; Cao, X. Hot corrosion behavior of rare earth zirconates and yttria partially stabilized zirconia thermal barrier coatings. *Surf. Coat. Technol.* **2010**, *204*, 3652–3661. [[CrossRef](#)]
33. Gavendová, P.; Čížek, J.; Čupera, J.; Hasegawa, M.; Dlouhý, I. Microstructure modification of CGDS and HVOF sprayed CoNiCrAlY bond coat remelted by electron beam. *Procedia Mater. Sci.* **2016**, *12*, 89–94. [[CrossRef](#)]
34. Khanna, A.S.; Rathod, W.S. Development of CoNiCrAlY oxidation resistant hard coatings using high velocity oxy fuel and cold spray techniques. *Int. J. Refract. Met. Hard Mater.* **2015**, *49*, 374–382. [[CrossRef](#)]

